Received: 10 June 2024 | Revised: 19 October 2024 | Accepted: 20 October 2024

DOI: 10.1002/eqe.4263

RESEARCH ARTICLE

WILEY

Non-linear time history analyses of a rigid block isolated with unbonded fiber-reinforced elastomeric isolators (UFREIs): A comparison between 3D finite element and phenomenological models

Hediyeh Sheikh[1] | **Gaetano Pianese**[2] | **Rajeev Ruparathna**[1] | **Niel C. Van Engelen**[1] | **Gabriele Milani**[2]

[1]Department of Civil and Environmental Engineering, University of Windsor, Windsor, Ontario, Canada

[2]Department of Architecture, Built Environment and Construction Engineering (ABC), Politecnico di Milano, Milan, Italy

Correspondence
Gaetano Pianese, Department of Architecture, Built Environment and Construction Engineering (ABC), Politecnico di Milano, Piazza Leonardo da Vinci 32, 20133 Milan, Italy.
Email: gaetano.pianese@polimi.it

Funding information
Natural Sciences and Engineering Research Council of Canada, Grant/Award Numbers: RGPIN-2019-03924, RGPIN-2019-04332

Abstract

Numerical modeling represents a pivotal tool in the seismic analysis and design of structural systems, enabling the detailed prediction and examination of structural responses under seismic loading. This research conducts a comparative analysis of two numerical modeling approaches aimed at simulating the seismic response of unbonded fiber-reinforced elastomeric isolators (UFREIs). The research focuses on a finite element (FE) model developed using Abaqus and a developed phenomenological model implemented in OpenSees, outlining the development and calibration processes for each. The FE model is developed based on simple rubber material testing data, while the phenomenological model is calibrated using experimental results from cyclic shear tests conducted on the UFREI device and the FE model. The primary objective of this study is to assess the effectiveness of these modeling approaches in predicting UFREI behavior under seismic conditions. This evaluation entails comparing model predictions with experimental data obtained from unidirectional shake table tests performed on a rigid block isolated by two UFREIs. This paper highlights the distinct advantages and limitations of each model in simulating UFREI dynamic responses during seismic events. Furthermore, it provides insights into the modeling techniques and discusses the computational demands and data requirements of each model, thereby aiding in their application to various aspects of seismic analysis and design.

KEYWORDS

finite element model, impact model, non-linear time history analysis, numerical fitting, phenomenological model, unbonded fiber-reinforced elastomeric isolators

1 | INTRODUCTION

Fiber-reinforced elastomeric isolators (FREIs) represent an innovative class of seismic isolators, distinct from traditional steel-reinforced elastomeric isolators (SREIs).[1,2] FREIs are characterized by their use of thin fiber layers rather than steel laminas for reinforcement. This shift not only significantly reduces the weight of the isolators but also facilitates production via cold vulcanization, a process that further decreases manufacturing costs. Cost efficiencies make seismic isolation systems more accessible, particularly in economically constrained settings, thereby expanding their use in regions and applications where they were previously unaffordable.[1,3] The reinforcement in FREIs can involve various types of fibers, such as glass,[4] Kevlar,[5] and carbon,[6] each contributing distinct properties to the isolators. FREIs can be implemented in several configurations depending on the needs of the structure and the specific seismic requirements: bonded (BFREI),[2] unbonded (UFREI),[7] and partially bonded (PBFREI).[8–10] The unbonded variant is particularly noteworthy; it operates without any bonding or mechanical fastening to the structure, relying on the friction between the isolator and the structural surfaces to transfer shear loads. This friction-based interaction, characterized by the so-called *rollover* lateral deformation, not only enhances damping capabilities but also decreases horizontal stiffness, which improves the overall seismic response of the structure compared to similar bonded designs.[11] These unique properties have attracted significant research interest, prompting investigations into their behavior and seismic performance. A considerable number of numerical and experimental studies have been conducted on UFREIs. Although the mechanical behavior of these devices is well-documented through both numerical and experimental studies, their application in real-world structures continues to be explored.[12] Numerical models, which serve as a cost-effective alternative to the production and experimental testing of these devices, are a valuable tool for the investigation of the seismic performance in structural applications. Nonetheless, the inherent non-linear behavior of these devices presents significant challenges in developing effective numerical models.[1,13]

The force-displacement relationship of an UFREI is characterized by softening and stiffening regimes. The softening region is characterized by a reduction in effective lateral stiffness due to rollover, resulting in a more efficient device by shifting the fundamental period further away from the critical high-energy range of typical earthquake events. This phenomenon (i.e., rollover) occurs when the end sections of the isolator lose contact with the upper and lower supports as lateral displacements are applied, shown in Figure 1A. The process of rollover continues until the initial vertical faces of the bearing rotate 90° and contact the supports, known as full rollover (Figure 1B). In the stiffening region, there is a gradual increase in effective stiffness, which acts as a self-restraint mechanism to prevent excessive displacements during extreme events.[14]

This study presents an in-depth comparison analysis of non-linear time history analyses performed using the finite element (FE) software Abaqus[15] and a phenomenological model implemented in OpenSees.[16] Specifically, experimental unidirectional shake table tests of a rigid block isolated with two UFREIs are modeled and analyzed using these two different numerical approaches, and the outcomes are evaluated against experimental results. The primary objective is to assess the capability of these numerical models to predict experimental outcomes accurately and to delineate the strengths and weaknesses of each approach, considering factors such as computational costs and the necessity for experimental tests in developing the numerical models. The numerical results are compared with experimental data using a procedure that allows for a detailed comparison, extending beyond, considering only the peak response. Additionally, given the tendency of these devices for slip instability, this research examines the ability of numerical models to predict such behavior.

The document is structured into six sections. Section 2 offers an overview of the numerical models, with a particular emphasis on 3D FE and phenomenological models. Section 3 describes the devices and the setup characteristics of the

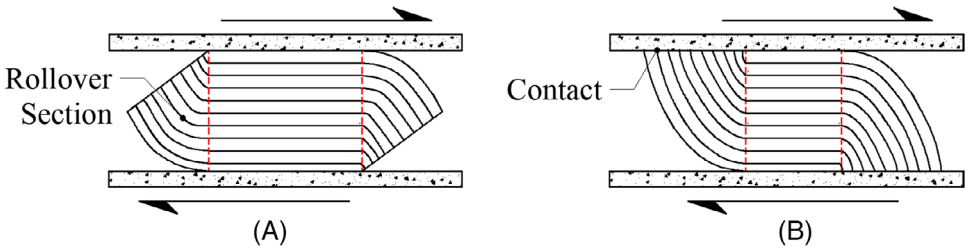

FIGURE 1 Lateral displacement of an UFREI illustrating (A) rollover and (B) full rollover. UFREI, unbonded fiber reinforced elastomeric isolator

experimental cyclic and shake table tests. Section 4 details the numerical models used in the study and the non-linear time history analyses performed. Section 5 includes a comprehensive discussion of the results obtained, focusing on the comparison of the considered numerical models and the experimental results. Finally, Section 6 presents the conclusions drawn from the study.

2 | BACKGROUND

2.1 | FE analysis

The utilization of FE models has proven to be a valuable tool for the design, characterization, and assessment of the seismic performance of FREIs. FE analysis offers significant advantages by reducing the need for costly experimental campaigns and allowing the exploration of a broader range of geometries and topologies. This method has been widely adopted for FREI preliminary investigations,[11,17,18] optimal design,[19,20] and fine-tuning of the lateral behavior.[21,22]

A commonly used approach for modeling FREIs involves employing a linear-elastic isotropic material model for the fiber reinforcement and a compressible hyperelastic constitutive model for the rubber material, such as the Neo-Hookean,[11,17] Ogden,[18] and Yeoh[23,24] models. These hyperelastic models are advantageous as they can be derived from the shear and bulk moduli of the elastomer. Numerous studies have validated this approach through both experimental[11,19,21] and analytical[22] results, highlighting its reliability for bonded and unbonded applications. Due to the limitations of hyperelastic models in capturing the energy absorption and the non-linear hysteretic behavior of FREIs, viscoelasticity has also been incorporated into the modeling. Das et al.[18] presented 3D FE models (FEM) for analyzing square FREIs under cyclic horizontal displacement and constant vertical load. The Ogden model was used to describe the hyperelastic behavior of the rubber, while the viscoelastic behavior was modeled using Prony's viscoelastic shear response parameters.[25,26] This model was validated with experimental UFREIs cyclic shear tests, confirming a strong correspondence with the observed mechanical properties and deformations. Dezfuli et al.[20] conducted a detailed parametric study on the different factors, such as the number and the thickness of rubber layers, as well as the thickness of carbon fiber reinforcing sheets, influencing the performance of rectangular carbon FREIs. The Mooney-Rivlin and Prony models were used for estimating the hyperelastic and viscoelastic behavior, respectively. The experimental tests on manufactured carbon FREIs were used for the calibration of the FE model. Subsequently, full-scale carbon FREIs were modeled and analyzed numerically. Ruano and Strauss[17] introduced advancements with a numerical model for unbonded carbon FREIs. The rubber pads in the models incorporated a phenomenological rheological model that blended hyperelastic and non-linear viscoelastic formulations. In particular, the rubber pads were modeled with Yeoh and the Bergstrom–Boyce non-linear viscoelastic models, calibrated using experimental rubber material tests, including uniaxial tensile, planar, and relaxation tests. The UFREI numerical model was validated with the experimental cyclic shear tests. Once validated, the study explored the effects of various parameters such as shape factor, aspect ratio, vertical pressure, and fiber orientation on stress distribution and mechanical properties.

The extensive adoption of FE models attests to their robustness and adaptability, significantly advancing the comprehension and innovation of UFREIs. While most studies based their FE models on experimental tests on bearings,[11,18–22] only one study predicted bearing performance using tests on elastomer materials.[17] This approach, discussed in this paper, can offer valuable insights during the preliminary design phase, allowing for a characterization of the devices without the need for prototype production and testing. This underscores another remarkable benefit of FE modeling. However, despite these advantages, the widespread integration of these models into numerical structural analyses can present practical challenges, primarily due to the substantial computational resources required for multiple FE UFREIs.[23,24] Consequently, a judicious approach is essential, balancing both the technical merits and computational feasibility.

2.2 | Phenomenological models

Several phenomenological models have been proposed to simulate the non-linear behavior of UFREIs subjected to dynamic loads. These models possess unique characteristics regarding their precision, computational efficiency, and the number and mechanical significance of the parameters utilized. Based on the type of equation used to calculate the restoring force, the hysteresis models of UFREIs can be classified as differential models that use differential equations to express the rate of variation of the force and displacement, and algebraic models that use mathematical equations to directly relate

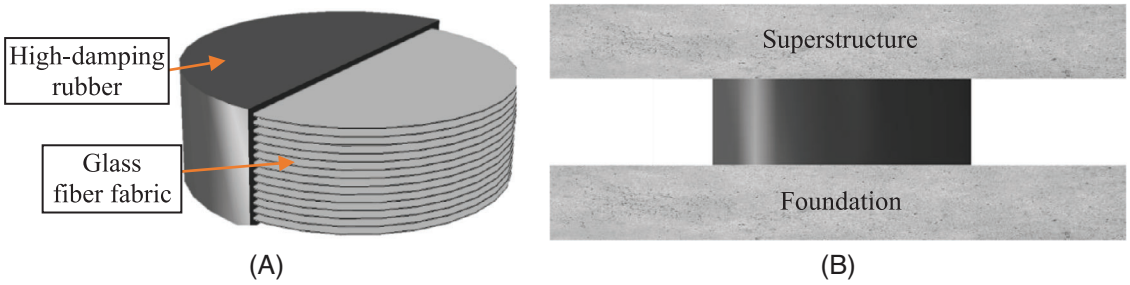

FIGURE 2 High-damping unbonded glass FREI: (A) section and (B) structural application. FREI, fiber-reinforced elastomeric isolator.

TABLE 1 Geometrical characteristics of the circular high-damping UFREIs.

Height (mm)	Base (mm)	Rubber thickness (mm)	Fiber thickness (mm)	n° rubber layers (–)	n° Fiber laminas (–)	Total rubber thickness (mm)
67.0	200	4	0.5	15	14	60

Abbreviation: UFREI, unbonded fiber-reinforced elastomeric isolator.

the force and displacement. Simplified bilinear and trilinear models,[27–29] are insufficient in capturing the more complex behavior commonly observed in UFREIs at larger shear strains.[30] Toopchi-Nezhad et al.[29] and Pianese et al.[31] utilized the Hwang et al.[32] model, which proved effective in predicting the response of SREIs under significant shear strains, to simulate the hysteretic behavior of UFREIs. This approach was supplemented by an iterative process for adjusting its parameters during non-linear time history analyses.

Nagarajaiah et al.[33] employed the widely adopted differential Bouc-Wen model[34,35] to simulate the behavior of SREIs under significant shear strains. Following this, Chen and Ahmadi,[36] Love et al.,[37] and Manzoori and Toopchi-Nezhad[38] developed modified versions of the Bouc-Wen model, tailored to accurately depict the hysteretic properties of both SREIs and UFREIs. Vaiana et al.[30] presented a novel algebraic model designed to replicate the rate-independent hysteretic behavior observed in mechanical systems and materials by resolving an algebraic equation.[30,39,40] Their model exhibited good accuracy in predicting the performance of UFREIs, particularly at low and intermediate displacements, and demanded less computational effort due to the absence of an ordinary differential equation (ODE) and a reduced number of parameters for fitting compared to traditional differential models such as Bouc-Wen models.

These models have demonstrated the ability to accurately predict hysteretic behavior at low and intermediate displacement levels (typically up to a shear strain of 150%).[30,38,41] To address the limitation of not fully aligning with experimental data at larger displacement levels beyond full rollover, an impact model (IM) was incorporated into the existing phenomenological models[13] (i.e., Bouc-Wen model with a fifth-order polynomial[38] and algebraic model[30]). The IM addressed this by accounting for energy dissipation during the contact between the elastomeric element and the supports, specifically during full rollover. The resultant hybrid model illustrated that integrating the impact model enhanced the effectiveness of current numerical models in capturing UFREI behavior at larger displacement amplitudes, particularly beyond full rollover.[13] Further validation results for the hybrid model, which involves incorporating the IM into the Bouc-Wen model with a fifth-order polynomial, and the algebraic model, encompassing both the cyclic test and the shake table test, can be referenced in Sheikh et al.[13]

3 | DEVICE PROPERTIES AND SHAKE TABLE TESTS

3.1 | Device geometric and mechanical properties

The isolators examined in this research were designed for the seismic isolation of low-rise masonry buildings.[42] These are UFREIs composed of alternating layers of high-damping rubber and glass fiber fabric. The primary geometrical characteristics of these devices are detailed in Figure 2 and Table 1. Prior to conducting shake table experiments, the isolators underwent cyclic shear testing at the Structural Engineering Laboratory of the University of Windsor, under a vertical pressure of 1.73 MPa and up to 200% shear strain. The outcomes of these tests, in terms of lateral stiffness (K_L), equivalent viscous damping (ξ), and the area enclosed within the hysteresis loops (W_s), are compiled in Table 2. Note that

TABLE 2 Cyclic shear test results.

Cycle (u/t_r)	K_L (kN/mm)	ζ_L (%)	W_s (kN mm)
0.25	0.52	10.7	79.1
0.50	0.41	9.97	232
0.75	0.34	9.85	431
1.00	0.29	9.84	661
1.50	0.24	10.8	1333
2.00	0.23	11.6	2422

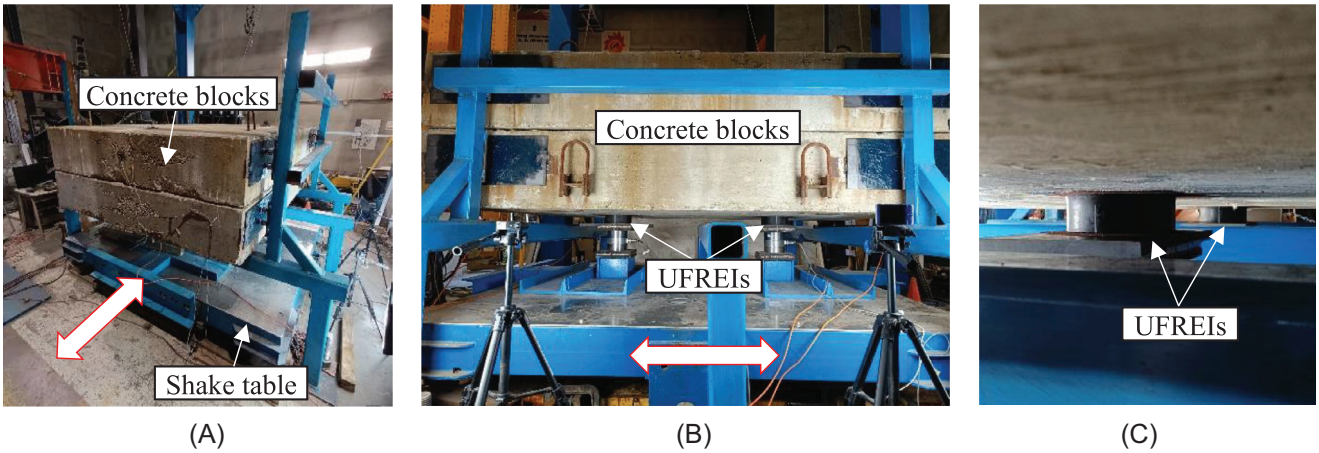

FIGURE 3 Shake table test setup: (A) experimental setup, (B) north-south view and (C) UFREI devices under the concrete blocks. UFREI, unbonded fiber-reinforced elastomeric isolator.

the devices underwent numerous compression and cyclic shear tests prior to this final characterization. Consequently, the final results slightly differ from those of an untested UFREI due to scragging and accumulated deterioration. These preliminary tests were vital for gaining an initial understanding of the behavior of the device and the expected performance in the shake table test. Additional information on the test program can be found in Pianese et al.[43] Furthermore, these tests played a key role in evaluating the accuracy of the 3D FEM in representing the mechanical properties of the isolators and in calibrating the analytical phenomenological model.

3.2 | Shake table tests

The experimental shake table tests were conducted at the Applied Dynamics Laboratory at McMaster University. The tests utilized a rigid block made from two concrete slabs, measuring 2.80 m x 2.00 m x 0.40 m and weighing around 110 kN (Figure 3). In this configuration a vertical pressure of 1.73 MPa was applied on each of the two high-damping UFREIs. The UFREIs were placed along the centerline of the block, spaced 1.30 m apart in the North-South direction (test direction). Given the unidirectional nature of the shake table tests, the out-of-plane motion of the rigid block was restricted using two reaction frames. The block was exposed to four distinct seismic ground motions selected from the earthquake database of Iran, encompassing the 1978 Tabas earthquake (peak ground acceleration (PGA) of 0.85 g at station TBS-A), the 1990 Manjil earthquake (PGA of 0.51 g at station ABB-A), the 2003 Bam earthquake (PGA of 0.81 g at station MAM), and the 2017 Sarpol earthquake (PGA of 0.52 g at station SPZ). Each ground motion was time-compressed by a factor of 2. This choice was made because the horizontal displacement of the actuator was limited to ± 130 mm and due to the table weight limitations, which resulted in relatively low axial loads and consequently a shorter period. To address these constraints, the authors devised a strategy involving time scaling of the original ground motions. This approach allowed for the investigation of the seismic behavior of the UFREIs under conditions of lower horizontal table displacement but higher accelerations. Furthermore, the acceleration was incrementally scaled from 0.10 g PGA up to the original PGA in 0.10 g increments. This incremental analysis allowed for a detailed evaluation of the response of UFREIs to different

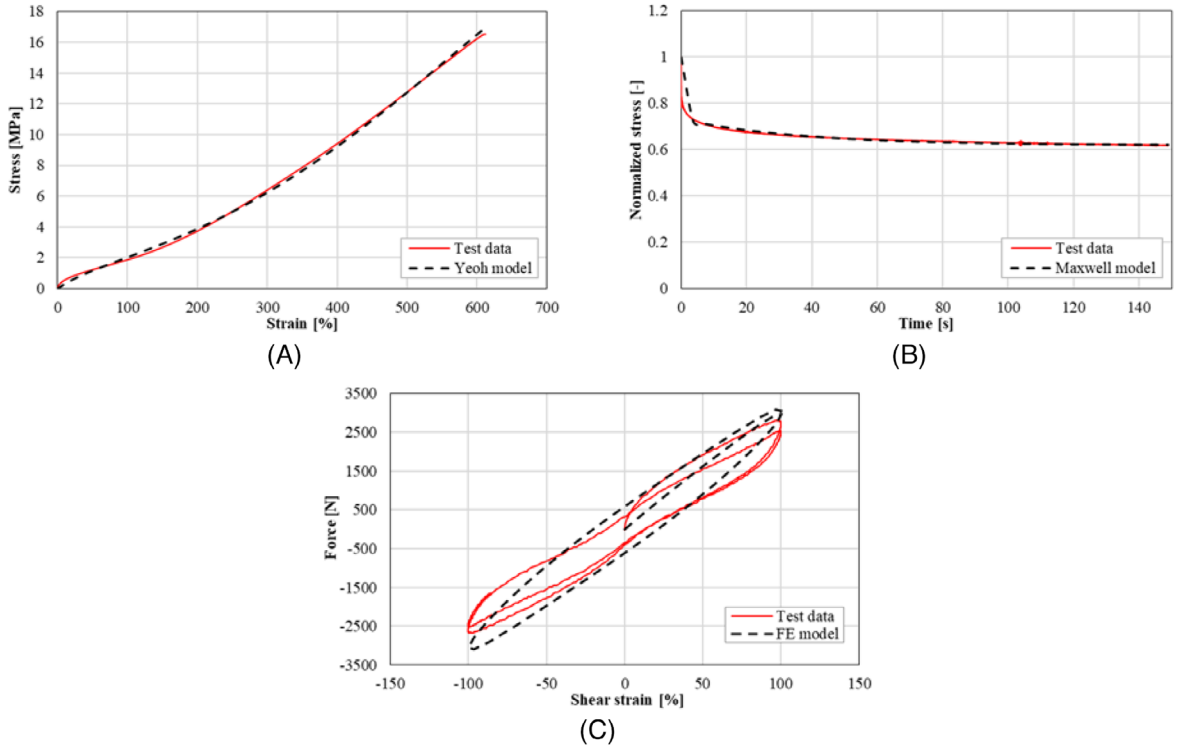

FIGURE 4 Comparison of the FEM and test data for the rubber compound: (A) uniaxial tensile test, (B) relaxation test, and (C) cyclic shear test. FEM, finite element model.

acceleration levels and ensured the safety of the test setup by identifying potential slips or damages. Further information about the performed experimental tests can be found in Pianese et al.[43] In this study, not all test scenarios were conducted numerically. Specifically, tests were selected at 0.20 g increments, starting at 0.10 g, until slip occurred. Additionally, for the numerical tests, records of shake table accelerations were utilized as input to ensure uniform external input across models, thereby enabling the results to be comparable to those obtained experimentally. Consequently, the actual PGAs listed in the following comparison tables slightly deviate from the expected precise increments of 0.2 g.

4 | NUMERICAL MODELS

4.1 | 3D FEM

4.1.1 | Calibration

The development of the 3D FE model was based on material tests performed on the rubber. Specifically, uniaxial tensile tests and relaxation tensile tests were utilized to derive the parameters for Yeoh and Maxwell's hyperelastic and viscoelastic models, respectively (Figure 4A,B). The quadruple shear test was considered for validation (Figure 4C). Details of this process are extensively documented in a previous work.[31] This approach is similar to the one proposed by Ruano and Strauss.[17] However, this study extends the investigation by exploring the seismic isolation prediction capability of the FE model, introducing a novel aspect to the research. Furthermore, the results from the FE model, derived from experimental tests on virgin rubber compounds, are compared with those from devices that have undergone prior compressive and cyclic shear testing, investigating the ability of the FE model to accurately reflect the actual conditions of the devices and evaluate any potential discrepancies.

To assess the accuracy of the proposed model, preliminary cyclic shear tests were replicated using the FE software Abaqus (Figure 5). The isolator was modeled using eight-node brick elements (C3D8RH) supported by two rigid supports. The bottom support was fixed, while the top was allowed free vertical and horizontal movement. No adhesive bond was defined between the supports and the rubber pad. Therefore, a penalty surface-interaction model (red area in Figure 5)

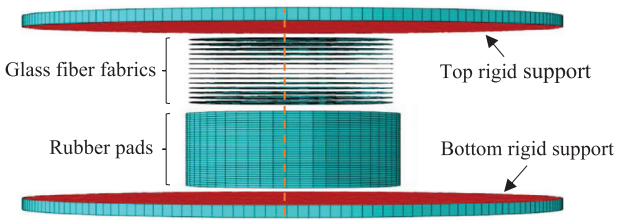

FIGURE 5 Exploded view of the 3D FEM of the UFREI for the numerical cyclic shear tests. FEM, finite element model; UFREI, unbounded fiber-reinforced elastomeric isolator.

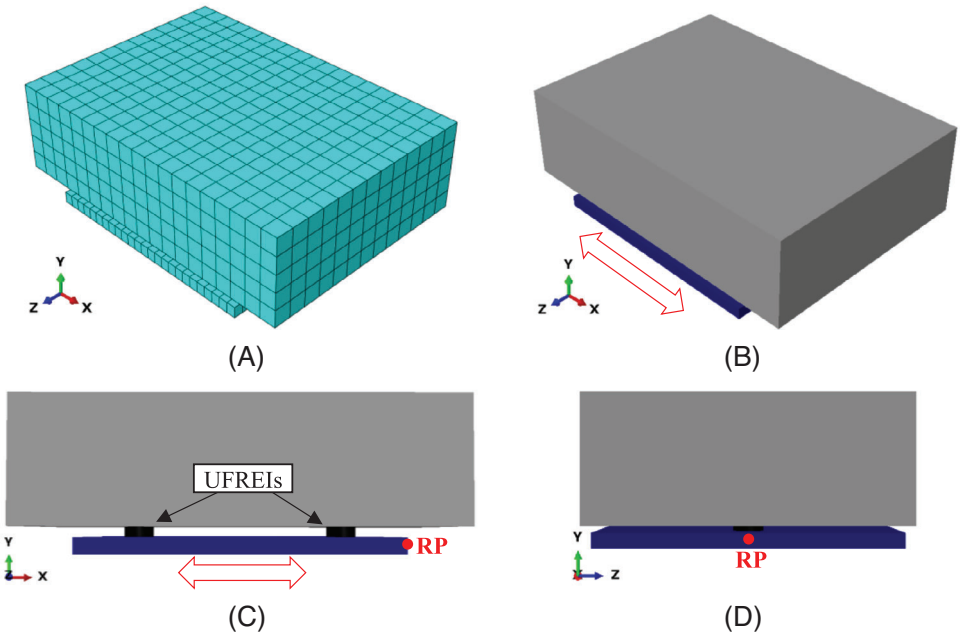

FIGURE 6 3D FEM in Abaqus for the shake table setup: (A) mesh, (B) XYZ, (C) XY and (D) YZ views. FEM, finite element model.

was implemented to simulate contact, with a friction coefficient (μ) set to 1.[44] The layers of glass fiber fabric within the rubber were modeled as embedded regions,[17] utilizing a 4-node doubly curved general-purpose shell, finite membrane strains. The fiber material was modeled with isotropic-elastic characteristics, having a Young's modulus (E) of 1500 MPa and a Poisson's ratio (ν) of 0.2.[45] The device was subjected to two full cycles of sinusoidal motion at a frequency of 0.5 Hz, experiencing strains ranging from 25% to 200%, under a vertical load of 1.73 MPa.

4.1.2 | Time history analysis

For the time history analyses, the setup of the experimental shake table tests was created in Abaqus, as shown in Figure 6. The isolators were modeled using the same methodology as applied in the cyclic shear tests. The shake table itself, situated at the base of the two UFREIs and depicted in dark blue in Figure 6, was modeled as a rigid body using 4-node 3D bilinear rigid quadrilateral mesh elements. The concrete blocks (shown in grey in Figure 6B–D) positioned above the two UFREIs were represented as a single element with a Young's modulus of 22,000 MPa, a Poisson's ratio of 0.2, and a density of 2.50×10^{-9} tonne/mm^3. This configuration ensured a vertical pressure of 1.73 MPa on the isolators. Given that the tests were unidirectional, the concrete block was constrained in the Y direction, while constraints on the shake table were applied in both the Y and Z directions. Acceleration time history inputs were applied to the reference point (RP) of the shake table along the X-axis. Similar to the approach in the cyclic shear tests, the interaction between the isolators and both the rigid block and the shake table was modeled using a penalty surface contact with a friction coefficient of 1. This

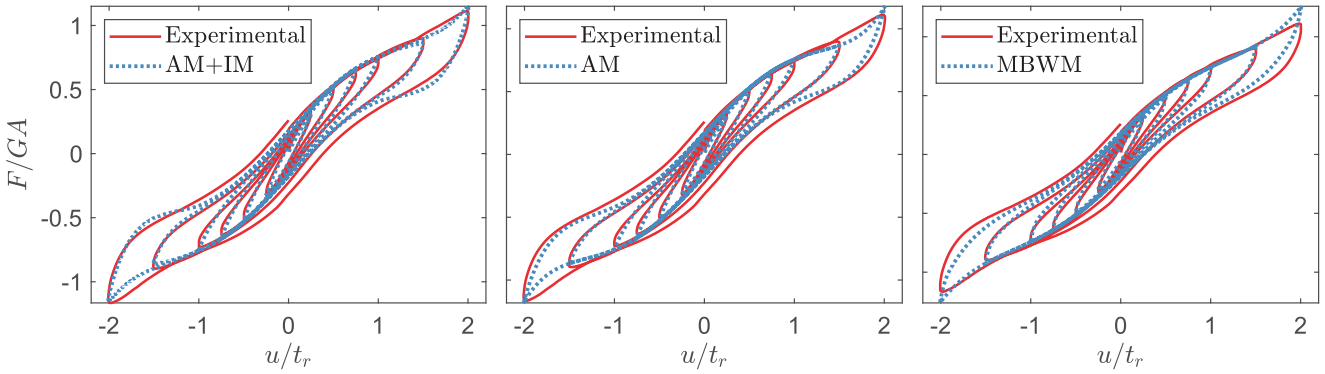

FIGURE 7 Comparison of the normalized experimental and numerical model hysteretic loops.

TABLE 3 MAE percentage of the model to reference ratio for all amplitudes.

	MAE (%)		
Model	K_L	ζ_L	W_s
MBWM	4.73	16.9	16.5
AM	3.39	14.2	16.5
AM+IM (Exp.)	3.07	13.3	13.7
AM+IM (FEM)	2.94	8.74	8.94

Abbreviations: AM, algebraic model; FEM, finite element model; IM, impact model; MAE, mean absolute error; MBWM, modified Bouc-Wen model.

value is commonly recommended[44]; however, it was found to be insufficient to prevent slip as will be discussed later in the paper.

4.2 | Phenomenological model

4.2.1 | Parameter fitting

The Bouc-Wen model, modified by including a fifth-order polynomial (MBWM),[36,37] the algebraic model (AM) proposed by Vaiana et al.,[30] and the impact model,[13] which has been incorporated to the AM (AM+IM), have been employed to validate and select a candidate model for use in time-history analysis.

The AM relies on a set of five parameters (k_a, k_b, α, β_1, and β_2) and defines a force-displacement hysteresis loop using four types of curves, and each parameter in the model influences the size and shape of the hysteresis loops in a specific way. Compared to other phenomenological models like the MBWM, the AM offers several advantages. The efficacy of the AM, along with its simplified implementation and reduced parameterization (i.e., only 5 parameters compared to 12 in the MBWM), make it a promising model for analyzing UFREIs. The IM, which includes a gap element, augments the predicted isolator force with the contact force when the displacement exceeds the initial contact threshold. The IM parameters (ξ, n, and λ) are added to the existing model parameters. All the model parameters need to be calibrated using experimental data; ξ is the damping constant, λ is a coefficient of the total thickness of elastomeric layers, t_r, and represents the displacement at the initial contact, and n captures the non-linear behavior. The inclusion of the IM is limited to the ultimate displacement of UFREIs, which is the point at which delamination/failure occurs or when the bearing loses lateral stability.

The model parameters utilized for simulating the hysteresis loops were derived through the calibration of numerical models to all cycle amplitudes simultaneously using the particle swarm optimization algorithm (PSO). The experimental test used for calibration was conducted immediately prior to the shake table investigation. This calibration process included minimizing the squared differences between the calculated and measured force during experimental testing. Figure 7 shows the comparison of the MBWM, AM, and AM+IM and the experimental hysteresis loops. The mean absolute error (MAE) of the model-to-experimental ratio for all amplitudes for K_L, ξ, and W_s for each model is presented in Table 3. The integration of the IM with the AM was conceptualized to capture hysteresis loops at larger displacements

TABLE 4 The model parameters used to simulate hysteresis loops with AM+IM.

Model	k_a	k_b	α	β_1	β_2	Ξ	n	λ
AM+IM (Exp.)	8.86×10^5	3.09×10^5	68.28	-2.55×10^7	1.21×10^9	1.70×10^5	1.17	1.00
AM+IM (FEM)	6.85×10^5	2.33×10^5	16.09	-1.79×10^7	1.26×10^9	6.83×10^3	1.18	1.35

Abbreviations: AM, algebraic model; FEM, finite element model; IM, impact model.

beyond full rollover. Previous studies[13,14] have indicated that the AM+IM demonstrates a significant reduction in prediction error compared to existing numerical models for UFREIs. However, due to the limited displacement capacity of the cyclic shear test setup, constrained to 2.0 t_r, the effectiveness of the IM in this context is not fully demonstrated. Regardless, the comparative analyses in Table 3 reveal that AM+IM outperforms the other models and has consequently been chosen for utilization in time history analysis.

The 3D FEM relies on fundamental rubber material testing data, while the AM+IM is calibrated using experimental cyclic shear tests. These models require varying computational demands. The FEM, while invaluable for designing and exploring geometric parameter effects on the lateral behavior of UFREIs, needs substantial computational costs in time history analyses, often taking several days to complete (depending on computer specifications). In contrast, simulations conducted using the AM+IM in OpenSees can be completed within minutes. However, it necessitates calibration through experimental cyclic shear tests for parameter identification. Therefore, considering that the FEM can be developed using straightforward rubber material tests, which are widely available in laboratories, an innovative approach is integrating these two models to leverage their respective strengths. The cyclic shear tests can be conducted by the FEM in Abaqus using rubber material test data, and subsequently, the AM+IM can be calibrated to the cyclic shear analysis data from the FEM. Table 4 shows the model parameters derived for simulating the hysteresis loops of the AM+IM fitted to experimental data (AM+IM (Exp.)) and the AM+IM fitted to FEM (AM+IM (FEM)). The MAE of the AM+IM (FEM) to the FEM outputs is also shown in Table 3.

4.2.2 | Time history analysis

The time history analysis was performed using OpenSees 3.4.0[16] in two dimensions. The OpenSees model was designed to match the characteristics of the experimental shake table test. The phenomenological model parameters obtained from the cyclic test (Table 4) were used in the time history analysis to represent the behavior of the considered UFREIs. The mass of the concrete block was evenly distributed between the two isolation devices. The experimental tests were conducted under a constant vertical load and the out-of-plane motion of the rigid block was restricted. Therefore, the rotational degrees of freedom at the isolators were held fixed, and these effects were not considered in the model. Consequently, the 2D model included an isolator element with a 3×3 stiffness matrix, featuring infinite axial and rotational stiffness but finite shear stiffness. The AM+IM was locally implemented as a uniaxial material object in OpenSees for analysis convenience.

5 | MODEL COMPARISON AND DISCUSSION

5.1 | Cyclic shear test

The three modeling approaches have been evaluated against the cyclic shear tests. The experimental data and the numerical models output for FEM, AM+IM (Exp.), and AM+IM (FEM) are presented in Figure 8. The model-to-experimental ratios for K_L, ξ, and W_s for the three approaches are shown in Table 5. The model-to-experimental ratio is a measure of the accuracy of the fitted model. The table reveals that the error in predicting the lateral effective stiffness by the AM+IM (Exp.) is minimal, approximately 3.10%, indicating the efficacy of the AM+IM in estimating the lateral stiffness. The MAE for ξ and W_s, considering all the displacement amplitudes, is 13.3% and 13.7%, respectively. However, the maximum error occurs at the lowest displacement level (0.25 t_r), a range typically surpassed by lateral displacement demands in practical isolation systems. In scenarios where the anticipated displacement demands are considerably lower, AM+IM fitting can be tailored to accommodate lower amplitude cycles, thereby enhancing the overall fit across all cases.

The 3D FEM exhibits a stiffer response compared to the actual device performance, with the MAE for K_L, ξ, and W_s, across all displacement amplitudes, equal to 20.8%, 18.3%, and 36.1%. Validation of FREI FEMs typically have errors

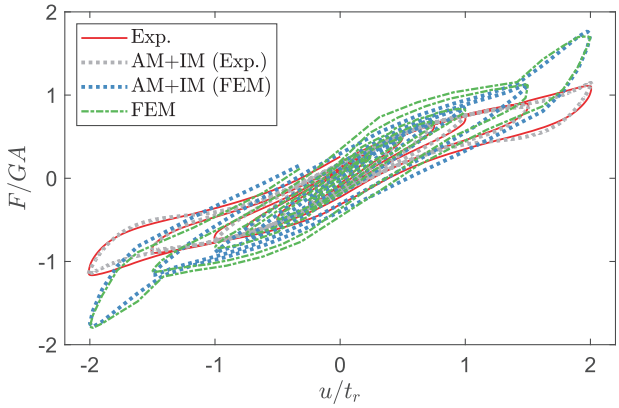

FIGURE 8 Comparison of the normalized hysteretic loops of experimental, 3D FEM, and AM+IM fitted to experimental and FEM data. AM, algebraic model; FEM, finite element model; IM, impact model.

TABLE 5 The model-to-experimental ratio for K_L, ξ, and W_s.

	FEM			AM+IM (Exp.)			AM+IM (FEM)		
Cycle (u/t_r)	K_L	ζ_L	W_s	K_L	ζ_L	W_s	K_L	ζ_L	W_s
0.25	0.82	0.51	0.41	0.97	0.73	0.71	0.85	0.51	0.45
0.50	0.98	0.78	0.75	1.03	1.05	1.08	1.01	0.63	0.74
0.75	1.08	0.96	1.02	1.05	1.13	1.18	1.13	0.87	0.74
1.00	1.15	1.07	1.22	1.03	1.13	1.17	1.20	1.00	1.18
1.50	1.26	1.26	1.57	0.96	1.03	0.99	1.28	1.14	1.44
2.00	1.57	0.98	1.52	1.01	0.82	0.91	1.57	0.93	1.44
MAE (%)	20.8	18.3	36.1	3.07	13.3	13.7	22.3	20.1	35.7

Abbreviations: AM, algebraic model; FEM, finite element model; IM, impact model; MAE, mean absolute error.

between 5% and 10%.[11,17,20] This disparity is anticipated because the model is based on material tests performed on a virgin rubber material. Therefore, the numerical model is a representation of an ideal untested UFREIs and doesn't consider the degradation of the rubber compound. As mentioned before, the experimental cyclic shear test used for calibration of the phenomenological model was performed on the devices after an experimental campaign that involved several compression and cyclic shear tests. So, this justifies the stiffer and less damped behavior of a virgin device compared to the real tested one. It is imperative to acknowledge the potential to fine-tune the accuracy of the FEM through calibrating the Yeoh and Maxwell parameters with UFREI experimental data.[44] However, for the scope of this research, the model was utilized in its initial form. The primary objective was to evaluate the ability of the FEM, developed solely from material tests, to predict the seismic performance of the device. This highlights the potential utility of the model in preliminary design evaluations.

Since the AM+IM (FEM) is calibrated to match the FEM analysis data, it exhibits comparable errors to the FEM outputs with respect to experimental data. The MAE for K_L, ξ, and W_s, across all displacement amplitudes, is 22.3%, 20.1%, and 35.7% for AM+IM (FEM), respectively.

5.2 | Time history analyses

5.2.1 | Stable response

The numerical model outputs of the non-linear time history analyses were evaluated with experimental data, based on the horizontal acceleration, displacement, and force time histories. For each earthquake record, the first three peak values were selected for comparison. The numerical models to the experimental ratio for each peak were calculated. Additionally, to assess the general trend over time, the running root mean square (RMS) of the displacement, force, and acceleration using a 1 s window were used to compare the estimation error of the models to experimental data, as shown in Figure 9.

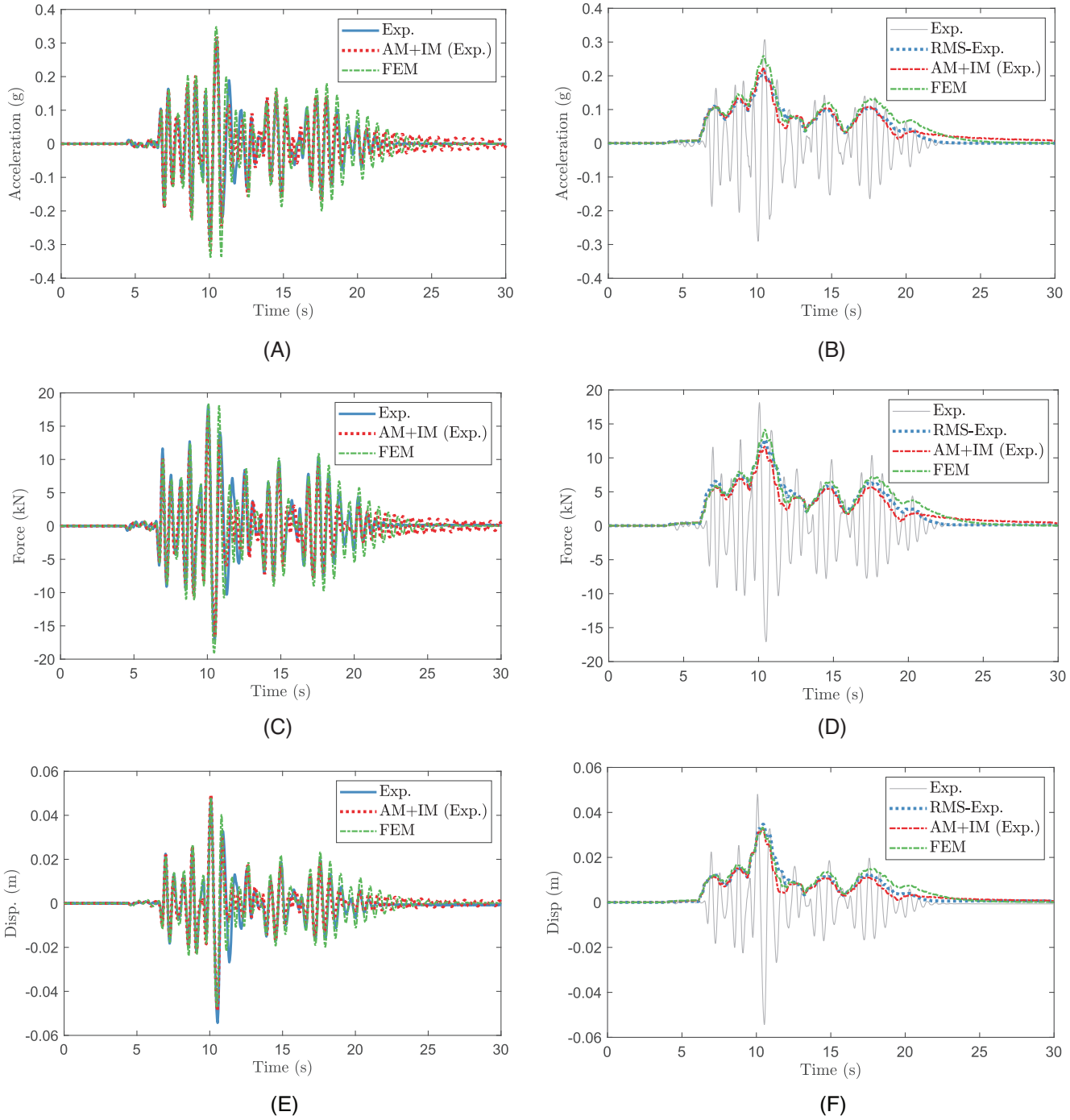

FIGURE 9 Non-linear time history results for the Tabas test at 0.50 g: (A,B) comparison of the acceleration, (C,D) force, and (E,F) displacement.

Although peak values are typically the primary focus, analyzing the running RMS provides insight into the overall model fit across all signal amplitudes and their variation over time.[13] As an example, Figure 9 shows the time history acceleration, displacement, force, and the corresponding running RMS plots using a 1 s window for the Tabas 0.5 g ground motion test. The quality of the fit of the running RMS plots is measured by the RMS error. This error is quantified as a scalar value, representing the average magnitude of errors within a given set of predictions. The RMS error shares the same physical units as the running RMS plots. However, for a more effective comparison, the RMS error for each time history is normalized against the peak value of the experimental RMS signal, yielding the normalized RMS (NRMS). The numerical and experimental results are presented in Tables 6–8, respectively, for the horizontal displacement, force, and acceleration.

TABLE 6 Comparison of the numerical displacement results and the experimental ones.

Ground motion	PGA (g)	FEM					AM+IM (Exp.)					AM+IM (FEM)				
		Model/Exp. Ratio for peaks			MAE (%) of peaks	NRMS	Model/Exp. Ratio for peaks			MAE (%) of peaks	NRMS	Model/Exp. Ratio for peaks			MAE (%) of peaks	NRMS
		1	2	3			1	2	3			1	2	3		
Bam	0.11	1.42	1.72	1.48	53.8	0.50	1.28	1.32	1.33	31.1	0.31	1.69	2.29	1.63	86.7	1.14
	0.34	1.02	1.04	0.97	3.20	0.06	0.84	1.00	0.72	15.1	0.12	1.13	1.13	1.04	9.90	0.15
	0.40	0.97	0.87	1.17	11.1	0.04	1.00	0.94	0.98	2.69	0.08	1.02	0.94	1.03	3.87	0.04
	0.57[a]	0.92	0.93	1.00	4.87	0.09	1.00	0.98	1.32	11.6	0.08	0.97	1.02	1.30	11.7	0.09
Tabas	0.11	2.13	1.25	0.72	55.6	0.58	1.94	1.85	1.08	62.1	0.72	2.04	1.15	0.77	47.6	1.52
	0.39	1.04	1.09	1.11	7.60	0.10	1.03	0.90	0.84	9.58	0.05	0.93	1.10	1.20	12.1	0.16
	0.55	0.86	1.00	1.23	12.2	0.06	0.90	1.02	0.93	6.64	0.06	0.86	0.92	1.21	14.2	0.16
	0.66	1.01	1.19	1.30	16.7	0.14	0.98	1.06	0.91	5.48	0.10	0.85	0.95	1.18	12.8	0.16
	0.76[a]	0.84	1.05	0.49	24.1	0.15	1.03	1.08	0.70	13.8	0.13	0.84	0.98	0.50	22.7	0.17
Manjil	0.10	1.02	1.42	1.29	24.5	0.50	0.57	0.84	0.55	34.6	0.71	1.57	1.77	1.83	72.0	1.76
	0.25	1.51	0.52	1.56	51.4	0.51	1.05	0.48	1.08	21.7	0.42	1.87	1.25	1.41	51.0	0.49
	0.51	0.52	0.91	1.75	43.7	0.65	1.11	0.94	1.22	12.9	0.21	1.31	1.44	1.36	37.1	0.68
Sarpol	0.13	0.92	1.00	1.22	10.1	0.14	1.46	1.23	1.29	32.6	0.27	1.05	1.50	1.38	31.2	0.70
	0.27	1.20	1.21	1.27	22.7	0.13	1.05	1.08	1.04	5.60	0.08	1.37	1.34	1.48	39.9	0.28
	0.54	1.10	1.10	1.23	14.3	0.09	0.88	1.00	0.79	11.0	0.09	1.19	1.05	1.20	14.8	0.14
MAE^1 (%)		22.7	18.9	29.5	23.7	24.9	18.6	17.0	19.6	18.4	22.9	32.0	28.3	33.3	31.2	51.0
MAE^2 (%)		15.9	13.1	28.7	19.3	18.3	6.20	9.10	16.4	10.6	12.8	22.3	13.9	26.6	20.9	23.0

Abbreviations: AM, algebraic model; FEM, finite element model; IM, impact model, MAE, mean absolute error; PGA, peak ground acceleration; NRMS, normalized root mean square.

[a]The tests in which slip occurred.

The MAE of the three peaks within each amplitude is also calculated and included in the tables to facilitate comparison. Additionally, the last two rows of each table show the MAE of each column; MAE^1 represents the mean absolute error percentage across all PGA amplitudes and ground motions, while MAE^2 represents the mean absolute error percentage across all PGA amplitudes and ground motions excluding the lowest PGA amplitude in each ground motion set.

The considered models encountered challenges in accurately capturing the behavior of the devices at the lowest PGA amplitude (approximately 0.10 g), that is indicative of low shear strain. This was expected for both models. The FEM showed differences in stiffness and damping during cyclic shear tests at low displacements. In the case of the phenomenological models, previous studies have demonstrated that it is less accurate at lower amplitudes.[13,14] Note that since the values involved in the lowest amplitudes are very small, it results in relatively large percent errors, which inaccurately represent the significance of the error in relation to the magnitude of the values being measured. Therefore, MAE^2 was defined to address this issue.

The displacement MAE^1 value, as shown in Table 6, is 18.4% for the AM+IM (Exp.), 23.7% for the 3D FEM, and 31.2% for the AM+IM (FEM). However, when excluding the lowest PGA amplitude, the MAE^2 values decrease to 10.6%, 19.3%, and 20.9%, respectively. The force MAE^1 values, shown in Table 7, for the AM+IM (Exp.), 3D FEM, and AM+IM (FEM) are 12.9%, 18.6%, and 16.7%, respectively, while the force MAE^2 values are 9.36%, 16.5%, and 14.8%. Similarly, the acceleration MAE^1 values, shown in Table 8, are 16.9%, 25.2%, and 25.2%, and the acceleration MAE^2 values are 10.8%, 25.5%, and 24.3% for the AM+IM (Exp.), 3D FEM, and AM+IM (FEM), respectively. In the 3D FEM analysis, unlike the horizontal forces and displacements, the acceleration MAE^2 does not show a reduction compared to MAE^1. This indicates that the FEM is less sensitive to accelerations. Anyway, considering MAE^2, the three modeling approaches demonstrated an acceptable ability to approximate the true behavior of the UFREIs during the shake table test. Specifically, the AM+IM (Exp.) exhibited an average estimation error of about 10%, while the 3D FEM and AM+IM (FEM) displayed an average estimation error of 20%. Overall, the FEM and the AM+IM (FEM) demonstrated consistently larger errors in comparison to the AM+IM (Exp.). Moreover, the three approaches exhibited discrepancies between the first and third peaks, with larger errors observed for the third peak in most of the PGA amplitudes. Notably, the first peaks showed smaller errors, highlighting the good fitting capacity of the models for capturing the peak response of the UFREIs. Considering the MAE^2 for the first peak, the AM+IM (Exp.) exhibited an average estimation error of about 7.6%, while the 3D FEM and AM+IM (FEM) showed about 17% and 18%, respectively. Note that a previous study[38] on a phenomenological model reported an average error of around 11.1% for the first peak of displacement and force compared with experimental shake table results. This value is higher than the average first peak error of displacement and force for the AM+IM (Exp.), which is 6.9%. For the FEM, to the best knowledge of the authors, no studies have been conducted on elastomeric bearings that compare experimental time-history results with FEMs. This gap in research makes it difficult to evaluate the observed 20% error margin. Nevertheless, given the initially larger errors in the cyclic shear tests (owing in part to the test history of the devices), these discrepancies in the seismic performance could be reduced to smaller values.

The MAE^2 values for NRMS of displacement, force, and acceleration average at 12% for the AM+IM (Exp.) and increase to 18% and 23% for the 3D FEM and AM+IM (FEM). These results indicate an acceptable overall agreement between the models and the experimental data, suggesting a consistent trend over time.

Note that in the phenomenological modeling approach (AM+IM) the accuracy of time history analysis results significantly relies on the precise calibration of model parameters utilized in the analysis. Since the experimental cyclic shear test, utilized for AM+IM model fitting, constituted the final assessment of shear behavior on the UFREIs before the shake table tests, it closely reflects the realistic behavior of the devices. Consequently, the AM+IM (Exp.), calibrated to this experimental data, exhibited notably smaller errors compared to the 3D FEM and to the AM+IM (FEM). The discrepancy observed in the errors between AM+IM (Exp.) and AM+IM (FEM) reflects the advantage of aligning model parameters with experimental shear test data when available. Moreover, the level of error observed in AM+IM (FEM), calibrated to the 3D FEM, remained consistent with the 3D FEM errors, emphasizing the feasibility of using this phenomenological model as an alternative to the FEM in structural analysis to lower computational costs.

Figure 10 shows hysteresis loops depicting the experimental, FEM, and the AM+IM (Exp.) outputs at both minimum (left) and maximum (right) PGA levels within a stable response domain (i.e., where no slip occurred). These plots further elucidate the challenges faced by numerical models in accurately capturing device behavior under very low accelerations and associated minimal horizontal displacements. Experimentally, the devices exhibited a more rigid response and greater damping capacity than predicted by simulations. Particularly at small displacements, the AM+IM (Exp.) demonstrated higher stiffness and damping compared to the FEM, suggesting a closer approximation to actual device behavior. However, at higher PGA levels, the models provided reasonably accurate depictions of device behavior, with the AM+IM (Exp.) consistently showing a better agreement. The comparison between the hysteresis loops obtained from AM+IM (FEM)

TABLE 7 Comparison of the numerical horizontal forces results and the experimental ones.

Ground motion	PGA (g)	FEM					AM+IM (Exp.)					AM+IM (FEM)				
		Model/Exp. Ratio for peaks			MAE (%) of peaks	NRMS	Model/Exp. Ratio for peaks			MAE (%) of peaks	NRMS	Model/Exp. Ratio for peaks			MAE (%) of peaks	NRMS
		1	2	3			1	2	3			1	2	3		
Bam	0.11	1.10	1.23	1.02	11.8	0.30	1.06	1.10	1.01	5.50	0.22	1.17	1.46	1.03	21.7	0.68
	0.34	1.06	1.09	1.13	9.36	0.09	0.87	0.79	0.97	12.5	0.11	1.08	1.09	1.13	10.0	0.16
	0.40	1.13	1.13	1.28	18.2	0.11	0.95	0.94	0.97	4.78	0.09	1.13	1.12	1.22	15.5	0.09
	0.57[a]	1.17	1.02	1.27	15.4	0.21	1.13	0.93	1.12	10.6	0.08	1.25	1.05	1.32	20.6	0.18
Tabas	0.11	0.82	1.34	0.48	34.8	0.28	1.33	1.55	0.81	35.7	0.40	0.69	0.45	1.39	41.8	0.71
	0.39	1.00	1.03	1.12	4.83	0.08	0.96	0.87	0.86	10.5	0.06	0.98	0.85	1.07	8.28	0.24
	0.55	1.01	1.12	1.29	14.0	0.07	0.92	0.98	0.92	5.89	0.07	0.88	1.07	1.15	11.1	0.20
	0.66	1.18	1.16	1.42	25.4	0.16	0.95	0.95	0.91	6.46	0.11	1.05	0.95	1.18	9.08	0.18
	0.76[a]	1.12	1.11	0.63	20.2	0.18	1.05	0.97	0.63	15.0	0.13	1.10	1.01	1.16	8.88	0.21
Manjil	0.10	0.62	0.82	0.89	22.5	0.19	0.42	0.57	0.76	41.8	0.42	1.00	1.12	1.06	5.84	0.75
	0.25	0.83	1.16	1.18	17.2	0.24	1.11	0.90	0.82	12.8	0.29	1.29	0.99	1.50	26.6	0.61
	0.51	0.48	0.80	1.45	39.2	0.42	0.97	0.88	1.10	8.57	0.14	1.11	1.24	1.68	34.6	0.38
Sarpol	0.13	0.69	0.81	0.68	27.4	0.07	1.19	0.99	1.03	7.67	0.16	0.70	0.89	0.84	19.0	0.37
	0.27	0.96	1.13	1.04	6.78	0.08	0.93	1.04	0.94	5.50	0.06	0.95	1.15	1.10	9.95	0.25
	0.54	1.01	1.19	1.14	11.3	0.07	0.90	0.96	0.82	10.4	0.06	0.97	1.13	1.08	8.09	0.18
MAE^1 (%)		16.0	15.2	24.5	18.6	17.0	13.4	13.1	12.2	12.9	16.1	13.5	15.3	21.4	16.7	34.5
MAE^2 (%)		12.9	12.2	24.5	16.5	15.6	7.56	8.01	12.5	9.36	11.0	11.2	9.7	23.4	14.8	24.3

Abbreviations: AM, algebraic model; FEM, finite element model; IM, impact model, MAE, mean absolute error; PGA, peak ground acceleration; NRMS, normalized root mean square.

[a]The tests in which slip occurred.

TABLE 8 Comparison of the numerical acceleration results and the experimental ones.

Ground motion	PGA (g)	FEM					AM+IM (Exp.)					AM+IM (FEM)				
		Model/Exp. Ratio for peaks			MAE (%) of peaks	NRMS	Model/Exp. Ratio for peaks			MAE (%) of peaks	NRMS	Model/Exp. Ratio for peaks			MAE (%) of peaks	NRMS
		1	2	3			1	2	3			1	2	3		
Bam	0.11	1.17	1.35	1.12	21.5	0.35	1.18	1.26	1.15	19.5	0.27	1.29	1.67	1.18	38.0	0.79
	0.34	1.18	1.19	1.21	19.3	0.12	1.05	0.96	0.91	5.89	0.09	1.22	1.24	1.24	23.7	0.21
	0.40	1.17	1.23	1.34	24.9	0.16	1.02	1.05	1.06	4.40	0.09	1.21	1.25	1.34	26.5	0.16
	0.57[a]	1.55	1.19	1.50	41.3	0.26	1.38	1.13	1.26	25.5	0.11	1.51	1.28	1.47	42.1	0.25
Tabas	0.11	0.90	1.45	0.59	31.9	0.31	1.52	1.74	0.88	46.0	0.50	0.78	1.54	0.52	41.5	0.83
	0.39	1.07	1.12	1.18	12.4	0.09	1.07	0.98	0.96	4.06	0.06	0.93	1.12	1.20	12.8	0.10
	0.55	1.13	1.16	1.49	26.0	0.09	1.03	1.10	1.09	7.37	0.06	1.11	1.04	1.37	17.4	0.24
	0.66	1.23	1.30	1.68	40.3	0.20	1.03	1.10	1.08	7.15	0.09	1.13	1.10	1.40	21.0	0.22
	0.76[a]	1.17	1.23	0.71	22.9	0.20	1.13	1.12	0.73	17.3	0.11	1.18	1.16	0.82	17.3	0.24
Manjil	0.10	0.67	0.89	0.77	22.5	0.21	0.47	0.64	0.41	49.6	0.48	1.12	1.19	1.27	19.3	0.87
	0.25	1.14	0.52	1.28	29.7	0.29	0.89	0.65	0.92	18.0	0.35	1.39	1.07	1.67	37.6	0.40
	0.51	0.53	0.89	1.62	40.3	0.50	1.04	1.01	1.28	11.1	0.20	1.08	1.48	1.49	34.9	0.48
Sarpol	0.13	0.73	0.87	0.76	21.5	0.06	1.30	1.12	1.19	20.3	0.21	0.76	0.93	1.05	12.0	0.07
	0.27	1.16	1.01	1.07	8.06	0.10	1.12	1.09	1.08	9.72	0.08	1.23	1.23	0.85	20.4	0.03
	0.54	1.19	1.16	1.10	15.1	0.09	1.01	1.09	1.14	7.95	0.07	1.19	1.17	1.04	13.2	0.08
MAE^1 (%)		22.3	21.5	31.7	25.2	20.0	16.8	17.1	16.9	16.9	18.4	21.4	24.0	30.2	25.2	33.2
MAE^2 (%)		22.5	19.9	34.1	25.5	18.9	8.95	9.93	13.4	10.8	11.8	21.2	19.4	32.2	24.3	21.9

Abbreviations: AM, algebraic model; FEM, finite element model; IM, impact model, MAE, mean absolute error; PGA, peak ground acceleration; NRMS, normalized root mean square.

[a]The tests in which slip occurred.

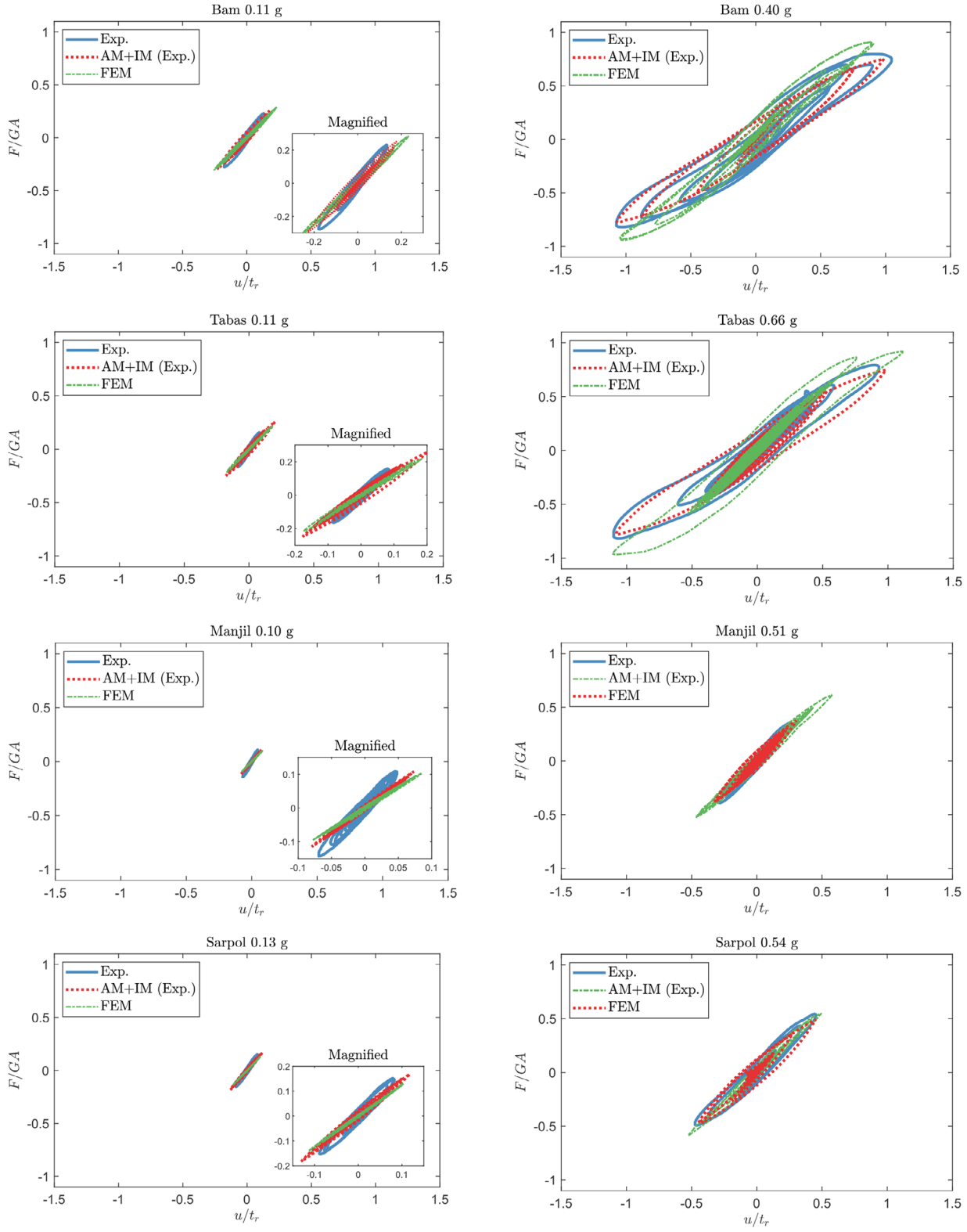

FIGURE 10 Comparison of horizontal shear strain versus horizontal forces curves for the tests in the domain of stable response at their minimum (left) and maximum (right) PGAs. PGA, peak ground acceleration.

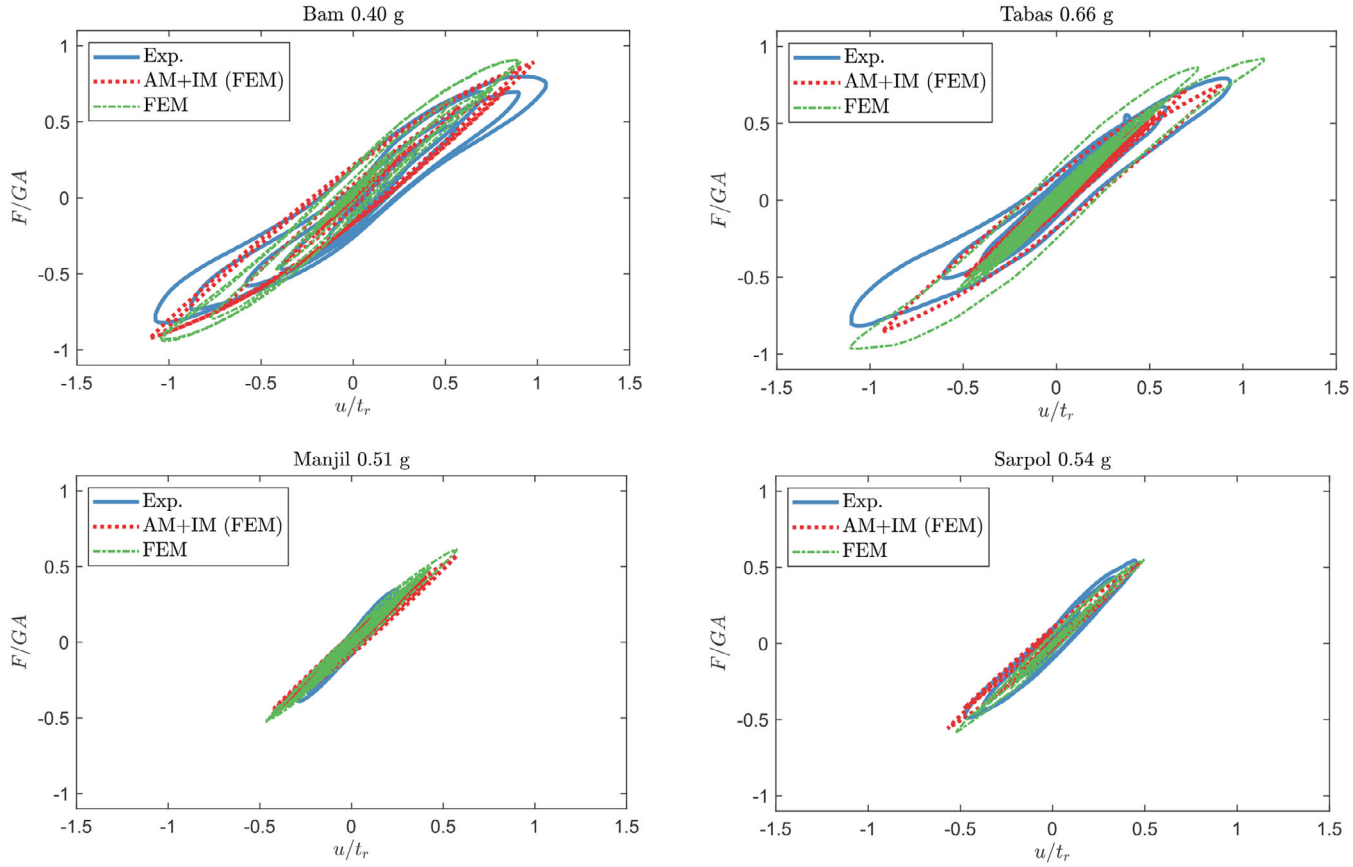

FIGURE 11 Comparison of horizontal shear strain versus horizontal forces curves of the maximum PGAs using the AM+IM (FEM) and FEM. AM, algebraic model; FEM, finite element model; IM, impact model; PGA, peak ground acceleration.

with FEM and experimental data at the maximum PGA level is also illustrated in Figure 11. When focusing solely on the maximum PGA levels (i.e., Bam 0.40 g, Tabas 0.66 g, Manjil 0.51 g, Sarpol 0.54 g), the average error for displacement, force, and acceleration peaks is 25.0%, 7.80%, and 19.0% for FEM, AM+IM (Exp.), and AM+IM (FEM), respectively. Notably, the AM+IM (Exp.) exhibited the lowest error and the AM+IM (FEM) demonstrated a closer alignment with experimental data compared to FEM. However, averaging across all amplitudes, both the AM+IM (FEM) and the FEM showed similar error levels.

5.2.2 | Unstable response

The comparison of numerical and experimental results was also extended to the domain of an unstable response, where slip occurred. Specifically, during the experimental shake table tests, the slip was observed in Tabas and Bam ground motions with PGAs of 0.76 g and 0.57 g, respectively. This behavior is challenging to predict, even with sophisticated models. The comparison for these two tests, as shown in Figure 12, reveals that the numerical models closely aligned with the experimental data in terms of displacements, and horizontal force, with average peak errors of 13.0% for the AM+IM (Exp.) and 16.0% for both FEM and the AM+IM (FEM). However, in terms of acceleration peak errors, this value rises to 21.0% for the AM+IM (Exp.), 32.0% for FEM, and 30.0% for the AM+IM (FEM), highlighting the models' greater sensitivity to slip occurrence when predicting accelerations.

Although the AM+IM (Exp.) aligns more closely with experimental results even in tests where slip occurred, it does not account for slip instabilities. In contrast, the 3D FEM can predict such occurrences. In fact, by modeling the setup and the interaction between the devices and the concrete blocks using a penalty surface contact and a friction coefficient that closely represents actual conditions, similar behavior could be achieved. In this study, the friction coefficient was set equal to 1 as is commonly recommended.[44] Nevertheless, the 3D FE model exhibited slip instability. In particular, due to the

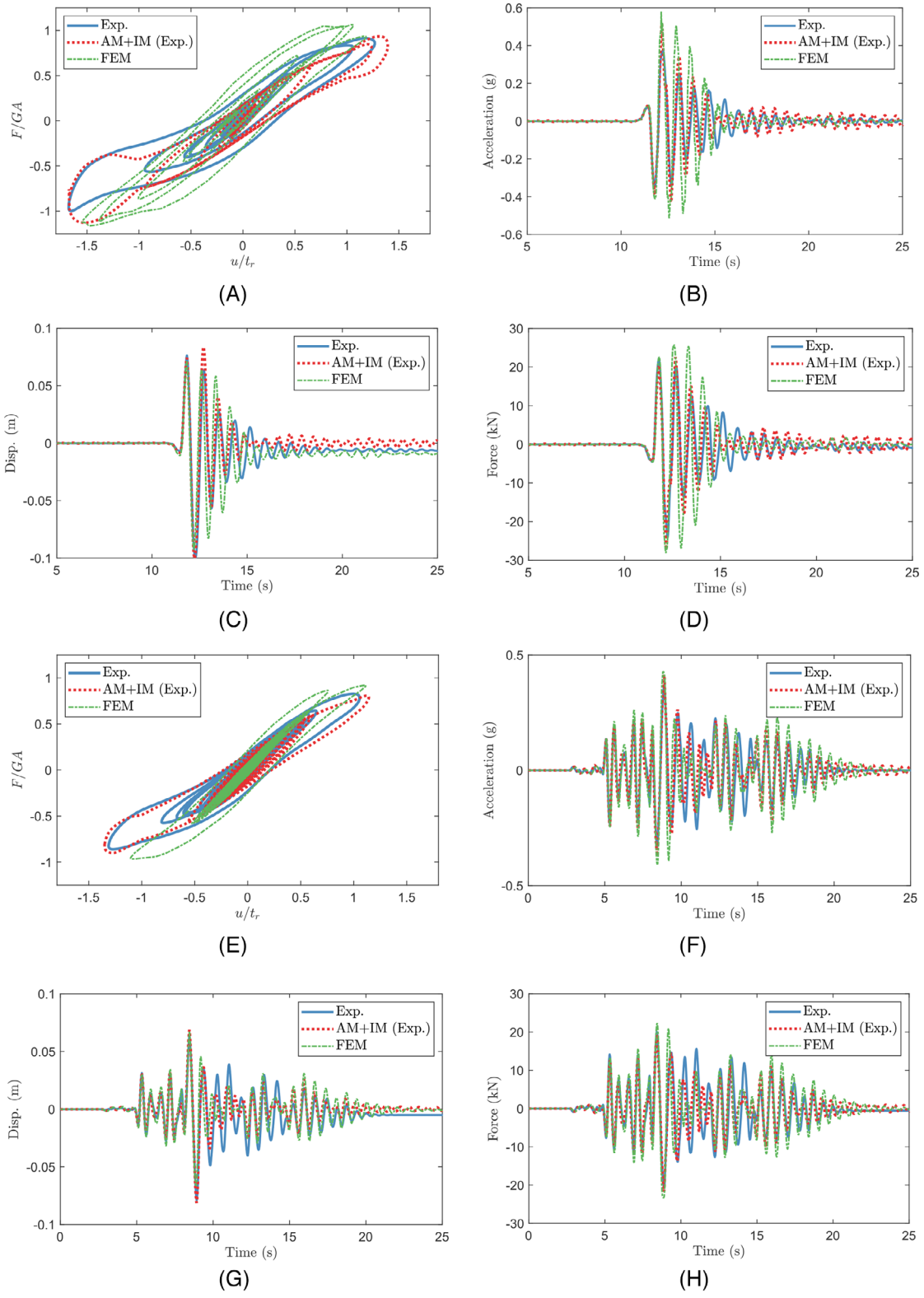

FIGURE 12 Comparison of the numerical and experimental results for the tests in the domain of unstable response: (A-B-C-D) Bam 0.57 g and (E-F-G-H) Tabas 0.76 g.

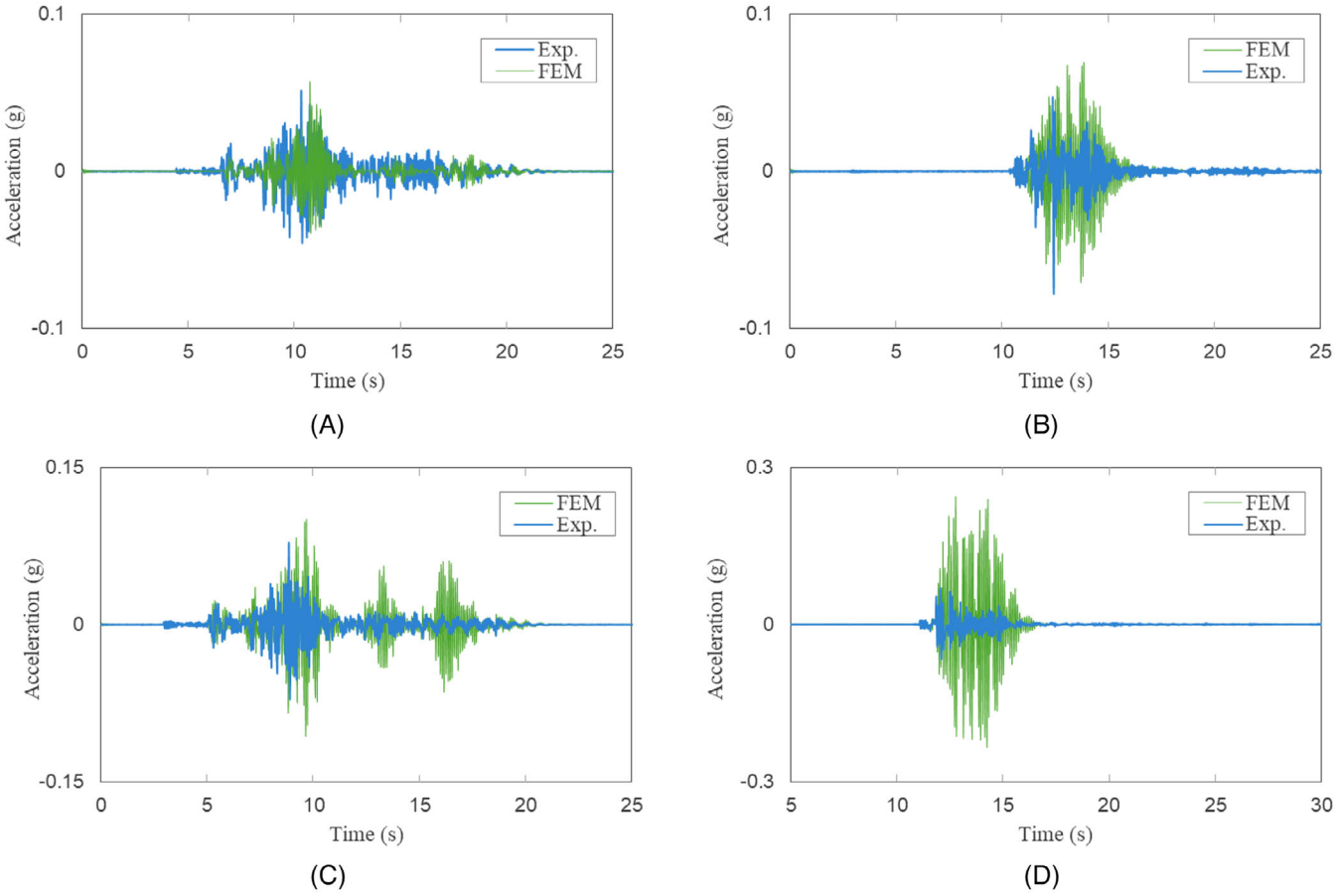

FIGURE 13 Comparison of FEM and experimental results in terms of vertical accelerations: (A) Tabas 0.55 g, (B) Bam 0.40 g, (C) Tabas 0.76 g, and (D) Bam 0.57 g. FEM, finite element model.

rocking motion of the concrete mass, a reduction of vertical pressure exerted on the devices occurred, allowing horizontal forces to exceed friction leading to slip instability. This phenomenon was also observed experimentally, highlighting the potential benefit of the FEM to capture the vertical performances and slip. Figure 13 presents a comparison of the vertical accelerations obtained from the FEM analysis and experimental measurements. Figure 13A and Figure 13B show the tests where no slip occurred, while Figure 13C and Figure 13D display tests where slip did occur. Although the discrepancies are smaller in the tests without slip, the FEM demonstrated limited accuracy in predicting vertical accelerations across all cases. Variations in setup modeling, friction coefficients, and device characteristics contributed to this discrepancy. Nonetheless, it remains crucial to highlight the opportunity to refine this model to mirror actual behavior more closely. Note, that the AM+IM model does not capture any vertical behavior. To include this, vertical experimental testing would be required and an appropriate model would need to be selected. Furthermore, an additional element would need to be included to capture sliding behavior.

6 | CONCLUSIONS

This study conducted an in-depth comparison analysis on two numerical models: A 3D FEM simulated in Abaqus and a phenomenological model (AM+IM) simulated in OpenSees software. The FEM was developed based on rubber material testing data, while the AM+IM parameters were calibrated through device cyclic shear tests. Despite the computational costliness of FEM compared to AM+IM, the latter required cyclic shear tests for parameter identification. To leverage their respective strengths, AM+IM was also calibrated to FEM shear test data. Consequently, three modeling approaches were considered for comparison: FEM, AM+IM calibrated to experimental shear tests (AM+IM (Exp.)), and AM+IM calibrated to FEM shear tests (AM+IM (FEM)). The study specifically examined the ability of the numerical models to accurately

predict outcomes from experimental shake table tests involving a rigid block isolated with two UFREIs. Evaluation of outputs from the numerical models involved comparing the first three peak values and the running RMS of horizontal displacement, force, and acceleration time histories against experimental data. Furthermore, the study investigated the ability of the models to predict slip instability, a common behavior in UFREIs, thus providing comprehensive insights into their predictive accuracy. The following conclusions were derived:

- Both numerical models faced challenges in accurately capturing behavior at the lowest PGA amplitude (PGA $\leq$ 0.15 g), indicative of low shear strain, with discrepancies in stiffness and damping observed at low displacements in cyclic shear tests.
- The AM+IM (Exp.) achieved smaller errors compared to the 3D FEM and AM+IM (FEM), particularly when excluding the lowest PGA amplitude.
- The three modeling approaches demonstrated acceptable agreement with experimental data. Specifically, averaging MAE^2 on displacement, force, and acceleration; AM+IM (Exp.) exhibited an average estimation error of about 10%, while the 3D FEM and AM+IM (FEM) displayed an average estimation error of 20%.
- The discrepancy in errors between AM+IM (Exp.) and AM+IM (FEM) underscored the importance of calibrating phenomenological model parameters to experimental shear test data, highlighting the advantage of aligning parameters with realistic behavior.
- While the 3D FEM exhibited a larger deviation in predicting the seismic response of the UFREIs, its independence from requiring cyclic shear test data for calibration makes it a viable option when such experimental data is unavailable. Also, the AM+IM (FEM) demonstrated a similar response to the FEM and is a faster and more suitable alternative in scenarios where experimental shear test data is lacking.
- Both models offered valuable insights into UFREI behavior during sliding instability. While the AM+IM (Exp.) aligned more closely with experimental results, even in tests where slip occurred, it does not account for slip instabilities, unlike the 3D FEM, which can predict such occurrences. However, further investigation is required to refine the FEM to better mirror actual sliding behavior.
- The AM+IM (FEM) offers a promising path forward, balancing the detailed insights gained from the FEM with the computational efficiency and experimental validation strengths of the phenomenological model, providing a comprehensive tool for both preliminary design and detailed structural analysis of UFREIs.

ACKNOWLEDGMENTS

The authors acknowledge the support of the Natural Sciences and Engineering Research Council of Canada (NSERC) [funding reference number RGPIN-2019-03924 and RGPIN-2019-04332]. The authors also thank the Structural Engineering Laboratory at the University of Windsor and the Applied Dynamic Laboratory at McMaster University for their support in conducting the experimental tests. Additionally, they extend their appreciation to Professor Michael Tait for his financial support and for granting access to his laboratory equipment during the shake table experiments.

DATA AVAILABILITY STATEMENT

The data that support the findings of this study are available from the corresponding author upon reasonable request.

ORCID

Hediyeh Sheikh https://orcid.org/0000-0002-7460-1234
Gaetano Pianese https://orcid.org/0000-0003-2700-2965
Niel C. Van Engelen https://orcid.org/0000-0002-3420-2028

REFERENCES

1. Van Engelen NC. Fiber-reinforced elastomeric isolators: a review. *Soil Dyn Earthquake Eng*. 2019;125:105621. doi:10.1016/j.soildyn.2019.03.035
2. Moon BY, Kang GJ, Kang BS, Kelly JM. Design and manufacturing of fiber reinforced elastomeric isolator for seismic isolation. *J Mater Process Technol*. 2002;130-131:145-150. doi:10.1016/S0924-0136(02)00713-6
3. Kelly JM, Naeim F. *Design of Seismic Isolated Structures: From Theory to Practice*. John Wiley & Sons; 1999. Published online.
4. Spizzuoco M, Calabrese A, Serino G. Innovative low-cost recycled rubber-fiber reinforced isolator: experimental tests and Finite Element Analyses. *Eng Struct*. 2014;76:99-111. doi:10.1016/j.engstruct.2014.07.001

5. Kelly JM, Takhirov SM, Analytical and Experimental Study of Fiber-Reinforced Elastomeric Isolators. In: R*ep No PEER 2001/11, Pacific Earthquake Engineering Research Center, University of California, Berkeley*; 2001.
6. Galano S, Losanno D, Calabrese A. Stability analysis of unbonded fiber reinforced isolators of square shape. *Eng Struct*. 2021;245:112846. doi:10.1016/j.engstruct.2021.112846
7. Habieb AB, Valente M, Milani G. Base seismic isolation of a historical masonry church using fiber reinforced elastomeric isolators. *Soil Dyn Earthquake Eng*. 2019;120:127-145. doi:10.1016/j.soildyn.2019.01.022
8. Van Engelen NC, Osgooei PM, Tait MJ, Konstantinidis D. Partially bonded fiber-reinforced elastomeric isolators (PB-FREIs). *Struct Control Health Monit*. 2015;22(3):417-432. doi:10.1002/stc.1682
9. Toopchi-Nezhad H, Ghotb MR, Al-Anany YM, Tait MJ. Partially bonded fiber reinforced elastomeric bearings: feasibility, effectiveness, aging effects, and low temperature response. *Eng Struct*. 2019;179:120-128. doi:10.1016/j.engstruct.2018.10.043
10. Van Engelen NC, Tait MJ, Konstantinidis D. Investigation of partially bonded fiber-reinforced elastomeric isolators (PB-FREIs) with nominal vertical tensile loads. *Can J Civ Eng*. 2019;46(8) 669–676. doi:10.1139/cjce-2018-0014
11. Toopchi-Nezhad H, Tait MJ, Drysdale RG. Bonded versus unbonded strip fiber reinforced elastomeric isolators: finite element analysis. *Compos Struct*. 2011;93(2):850-859. doi:10.1016/j.compstruct.2010.07.009
12. Thuyet VN, Deb SK, Dutta A. Mitigation of seismic vulnerability of prototype low-rise masonry building using U-FREIs. *J Perform Constr Facil*. 2018;32(2):04017146. doi:10.1061/(asce)cf.1943-5509.0001136
13. Sheikh H, Ruparathna R, Van Engelen NC. Implementation, Verification, and Validation of an Impact Model for Lateral Numerical Modeling of Unbonded Fiber-Reinforced Elastomeric Isolators. *J Struct Eng*. 2023;149(11):04023153. doi:10.1061/jsendh.steng-12541
14. Sheikh H, Ruparathna R, Van Engelen NC. Investigation of seismic fragility curves of unbonded FREIs: adaptive characteristics and modeling sensitivity. *Earthq Eng Struct Dyn*. 2024;53(5):1826-1840. doi:10.1002/eqe.4097
15. Smith M. *ABAQUS/Standard User's Manual, Version 6.9*. Dassault Systèmes Simulia Corp; 2009.
16. McKenna F, Scott MH, Fenves GL. Nonlinear finite-element analysis software architecture using object composition. *J Comput Civil Eng*. 2010;24(1):95-107.
17. Castillo Ruano P, Strauss A. Finite element analysis for nonlinear unbonded circular fiber-reinforced elastomeric bearings. *J Compos Sci*. 2021;5(7):170. doi:10.3390/jcs5070170
18. Das A, Dutta A, Deb SK. Performance of fiber-reinforced elastomeric base isolators under cyclic excitation. *Struct Control Health Monit*. 2015;22(2) 197–220. doi:10.1002/stc.1668
19. Osgooei PM, Tait MJ, Konstantinidis D. Finite element analysis of unbonded square fiber-reinforced elastomeric isolators (FREIs) under lateral loading in different directions. *Compos Struct*. 2014;113:164-173. doi:10.1016/j.compstruct.2014.02.033
20. Hedayati Dezfuli F, Alam MS. Sensitivity analysis of carbon fiber-reinforced elastomeric isolators based on experimental tests and finite element simulations. *Bull Earthquake Eng*. 2014;12(2):1025-1043. doi:10.1007/s10518-013-9556-y
21. Van Engelen NC, Osgooei PM, Tait MJ, Konstantinidis D. Experimental and finite element study on the compression properties of Modified Rectangular Fiber-Reinforced Elastomeric Isolators (MR-FREIs). *Eng Struct*. 2014;74:52-64. doi:10.1016/j.engstruct.2014.04.046
22. Tran C, Calabrese A, Vassiliou MF, Galano S. A simple strategy to tune the lateral response of unbonded Fiber Reinforced Elastomeric Isolators (FREIs). *Eng Struct*. 2020;222:111128. doi:10.1016/j.engstruct.2020.111128
23. Habieb AB, Formisano A, Milani G, Pianese G. Seismic performance of Unbonded Fiber-Reinforced Elastomeric Isolators (UFREI) made by recycled rubber. Influence of suboptimal crosslinking. *Eng Struct*. 2022;256:114038. doi:10.1016/j.engstruct.2022.114038
24. Habieb AB, Milani F, Milani G, Pianese G, Torrini D. Vulcanization degree influence on the mechanical properties of Fiber Reinforced Elastomeric Isolators made with reactivated EPDM. *Polym Test*. 2022;108:107496. doi:10.1016/j.polymertesting.2022.107496
25. Holzapfel GA. On large strain viscoelasticity: continuum formulation and finite element applications to elastomeric structures. *Int J Numer Methods Eng*. 1996;39(22):3903-3926. doi:10.1002/(SICI)1097-0207(19961130)39:22⟨3903::AID-NME34⟩3.0.CO;2-C
26. Chen T, *Determining a Prony Series for a Viscoelastic Material from Time Varying strain Data*. NASA Langley Technical Report Server; 2000.
27. Pauletta M, Cortesia A, Pitacco I, Russo G. A new bi-linear constitutive shear relationship for Unbonded Fiber-Reinforced Elastomeric Isolators (U-FREIs). *Compos Struct*. 2017;168:725-738. doi:10.1016/J.COMPSTRUCT.2017.02.065
28. Calabrese A, Spizzuoco M, Strano S, Terzo M. Hysteresis models for response history analyses of recycled rubber–fiber reinforced bearings (RR-FRBs) base isolated buildings. *Eng Struct*. 2019;178:635-644.
29. Toopchi-Nezhad H, Tait MJ, Drysdale RG. Simplified analysis of a low-rise building seismically isolated with stable unbonded fiber reinforced elastomeric isolators. *Can J Civ Eng*. 2009;7(36):1182-1194. doi:10.1139/L09-05
30. Vaiana N, Sessa S, Marmo F, Rosati L. An accurate and computationally efficient uniaxial phenomenological model for steel and fiber reinforced elastomeric bearings. *Compos Struct*. 2019;211(1):196-212. doi:10.1016/j.compstruct.2018.12.017
31. Pianese G, Van Engelen N, Toopchi-Nezhad H, Milani G. An experimental and numerical insight into the unbonded and partially bonded high-damping fiber-reinforced elastomeric isolators. *Soil Dyn Earthquake Eng*. 2024;187:109016. doi:10.1016/J.SOILDYN.2024.109016
32. Hwang J, Wu J, Pan T, Yang G. A mathematical hysteretic model for elastomeric isolation bearings. *Earthq Eng Struct Dyn*. 2002;31(4):771-789. doi:10.1002/eqe.120
33. Nagarajaiah S, Reinhorn AM, Constantinou MC. Nonlinear dynamic analysis of 3-D-base-isolated structures. *J Struct Eng*. 1991;117(7):2035-2054. doi:10.1061/(ASCE)0733-9445(1991)117:7(2035)
34. Bouc R Forced vibrations of mechanical systems with hysteresis. In: *Fourth Conference on Nonlinear Oscillations*, Prague, 5-9 September 1967.
35. Wen YK. Method for random vibration of hysteretic systems. *J Eng Mech Division*. 1976;102(2):249-263. doi:10.1061/JMCEA3.0002106

36. Chen Y, Ahmadi G. Wind Effects on Base-Isolated Structures. *J Eng Mech*. 1992;118(8):1708-1727. doi:10.1061/(ASCE)0733-9399(1992)118:8(1708)
37. Love J, Tait M, Toopchi-Nezhad H. A hybrid structural control system using a tuned liquid damper to reduce the wind induced motion of a base isolated structure. *Eng Struct*. 2011;33(3):738-746.
38. Manzoori A, Toopchi-Nezhad H. Application of an extended Bouc-Wen model in seismic response prediction of unbonded fiber-reinforced isolators. *J Earthquake Eng*. 2017;21(1):87-104. doi:10.1080/13632469.2016.1138166
39. de Gregorio D. Reformulation of a phenomenological model for symmetric rate-independent hysteresis. *Structures*. 2022;45:353-360. doi:10.1016/J.ISTRUC.2022.08.099
40. Vaiana N, Rosati L. Classification and unified phenomenological modeling of complex uniaxial rate-independent hysteretic responses. *Mech Syst Signal Process*. 2023;182:109539. doi:10.1016/J.YMSSP.2022.109539
41. Van Engelen NC, Konstantinidis D, Tait MJ. Structural and nonstructural performance of a seismically isolated building using stable unbonded fiber-reinforced elastomeric isolators. *Earthq Eng Struct Dyn*. 2016;45(3):421-439. doi:10.1002/eqe.2665
42. Pianese G, Van Engelen N, Toopchi-Nezhad H, Milani G. High-damping fiber-reinforced elastomeric seismic isolator in different boundary conditions: an experimental insight. *Eng Struct*. 2024;300:117199. doi:10.1016/j.engstruct.2023.117199
43. Pianese G, Van Engelen N, Tait M, Milani G. Shake table tests on a rigid block isolated with high-damping unbonded fiber-reinforced elastomeric isolators. *Structures*. 2024;64(106595):106595. https://doi.org/10.1016/j.istruc.2024.106595
44. Saremi E, Toopchi-Nezhad H. Finite element modeling of horizontal load-displacement hysteresis loops in unbonded elastomeric isolators. *Structures*. 2021;34:2987-2995. doi:10.1016/j.istruc.2021.08.095
45. Ghorbi E, Toopchi-Nezhad H. Annular fiber-reinforced elastomeric bearings for seismic isolation of lightweight structures. *Soil Dyn Earthquake Eng*. 2023;166:107764. doi:10.1016/J.SOILDYN.2023.107764

How to cite this article: Sheikh H, Pianese G, Ruparathna R, Van Engelen NC, Milani G. Non-linear time history analyses of a rigid block isolated with unbonded fiber-reinforced elastomeric isolators (UFREIs): A comparison between 3D finite element and phenomenological models. *Earthquake Engng Struct Dyn*. 2025;54:449–470. https://doi.org/10.1002/eqe.4263